ISSN 1054-660X, Laser Physics, 2010, Vol. 20, No. 7, pp. 1641–1646.

Laser-Induced Hydrodynamics in Water-Saturated Biotissues. 1. Generation of Bubbles in Liquid

V. I. Yusupov[a, b, *], V. M. Chudnovskii[a], and V. N. Bagratashvili[b]

[a] *Il'ichev Pacific Institute of Oceanology, Far East Division, Russian Academy of Sciences, Baltiiskaya ul. 43, Vladivostok, 690041 Russia*

[b] *Institute on Laser and Information Technologies, Russian Academy of Sciences, Pionerskaya ul. 2, Troitsk, Moscow oblast, 142190 Russia*

*e-mail: iouss@yandex.ru

Received January 21, 2010

Abstract—The hydrodynamic effects that are induced in water by the moderate-power (1–5 W) CW laser radiation delivered via an optical fiber are investigated. The effective hydrodynamic processes in water are related to the explosive boiling in the vicinity of the heated end surface of the fiber. The resulting bubbles with sizes ranging from several to several tens of microns have velocities of up to 100 mm/s in the vicinity of the end surface. The generation of bubbles in a capillary gives rise to the stable circulation of liquid with the period ranging from 0.2 to 1.0 s. The hydrodynamic effects under study can be employed in the surgical and regenerative procedures in biotissues.

DOI: 10.1134/S1054660X1014001X

INTRODUCTION

Modern laser medical technologies widely employ the delivery of laser radiation to the irradiated tissues via optical fibers. Optical fibers easily penetrate through needles and endoscopic channels, and lasers can be used for puncture and endoscopic operations [1, 2] including the procedures related to the treatment of connective tissues in cartilages, joints, and vertebral column (e.g., osteochondrosis, osteoporosis, arthritis, and arthrosis). One of the tendencies in the laser treatment of connective tissues lies in the application of the moderate-power (1–5 W) radiation. The examples of such technologies are fractional photothermolysis [3], laser engineering of cartilages [4], puncture multichannel laser decompression of disk [5, 6], laser intervention upon osteochondrosis [7], and the surgical treatment of the chronic osteomyelitis [8]. The fractional photothermolysis [3], which employs the radiation with a wavelength of 1.55 μm and a pulse energy of up to 10 mJ, allows the effective remodeling of skin due to the creation of multiple point damages in the tissue. The application of the controlled moderate-power laser radiation (1.55 μm and 2 W) makes it possible to modify the shape of cartilage (e.g., for the correction of nasal septum) [9, 10]. The method for the laser reconstruction of the intervertebral disk (ID) involves the delivery of the radiation with a wavelength of 1.55 μm and a power of up to 1 W through a quartz fiber to the ID [4]. The treatment of osteochondrosis is based on the formation of multiple channels in the ID using a quartz fiber with the carbon-coated end surface that is heated by the laser radiation with a wavelength of 970 nm and a power of 3 W [5–7]. In the procedures for the treatment of osteomyelitis, the laser channels are formed in the medullary tissue [8].

It is commonly accepted that the surgical destruction of lesion focus and the recovery of tissue in all of the above procedures result from the laser destruction and heating of tissues, which are provided by the local heating of the distal fragment of the optical fiber and the effective absorption of the laser radiation in water and tissues. However, in many cases, the developed therapeutic effect related to the moderate-power laser irradiation cannot be interpreted using only thermal effects, since most organs with connective tissues (e.g., disks and bones) are not heated by the laser irradiation (see, for example [5]). Evidently, the thermal destruction is insufficient to account for a sharp decrease in the density of herniation immediately after the laser manipulation that results in the transformation of hernia into a soft sponge, since the herniation is relatively far from the region of the channel formation. Note that the effect of the moderate-power laser radiation that induces the tissue regeneration [4–7] remains uninterpreted.

We assume that effective hydrodynamic processes serve as dominant factors in the surgical treatment of the diseases of musculoskeletal system (e.g., intervertebral hernia and osteomyelitis) using the laser puncture procedures. In this work, we study the biologically important hydrodynamic effects induced by the moderate-power laser radiation in the vicinity of the heated end surface of optical fiber in water, in particular, the generation of gas–vapor bubbles.

The interest in microbubbles and the generation of such objects has been driven by the prospects for practical applications in the systems for ultrasonic clean-

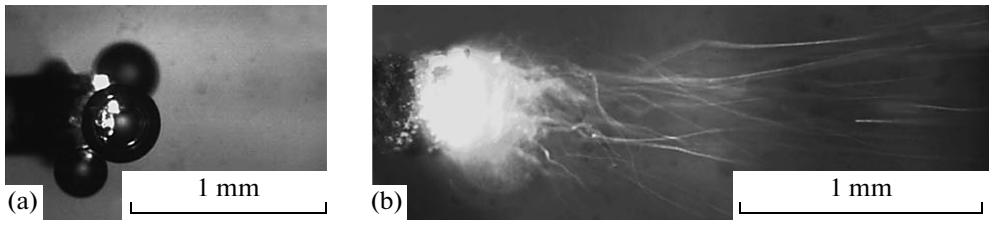

Fig. 1. The generation of microbubbles in the vicinity of the blackened end surface of the optical fiber in water for the laser radiation with a wavelength of 970 nm and a power of (a) 1 and (b) 5 W (the photograph is taken from above at an exposure time of 250 ms).

ing, ultrasonic analysis of biotissues, and lithotripsy [11]. Note the absence of data regarding the features of the laser-induced generation of bubbles in liquid in the vicinity of the heated end of the optical fiber in free liquid and in the liquid in capillary.

MATERIALS AND METHODS

We study the laser-induced hydrodynamic effects with the aid of the optical methods using a Plexiglas cell filled with water (the horizontal dimensions are 150 × 100 mm and the height is 15 mm) and glass capillaries with an inner diameter of 1 mm. In most experiments, the working end of the laser fiber is preliminary blackened due to a short (about 1 s) contact of the fiber with wood at a laser power of about 3 W. The end surface of the fiber appears coated with a thin carbon layer owing to the burning of wood. Such a procedure is well reproduced, so that from 10 to 20% of the laser energy is absorbed in the thin carbon layer. IRE–Polyus computer-controlled fiber lasers (LS-0.97 and LS-1.55 with wavelengths of 970 nm and 1.55 μm, respectively, and powers of 0–10 and 0–5 W, respectively) are interfaced with quartz fibers with a quartz core diameter of 400 μm. The fiber is fixed in the cell, which is placed on the worktable of a MICROS MC300 microscope equipped with a Vision digital color camera interfaced with PC. The cell can also be placed on the table with illumination from below, and the processes in the vicinity of the heated end of the fiber are recorded using a Photron Fastcam SA-3 camera at rates of 2000 or 10000 frames per second. To control the laser spectrum and power, we employ an Ocean Optics USB4000 fiber spectrum analyzer, which is interfaced with PC and has an optical resolution of about 1.5 nm and the working wavelength range 200–1100 nm, and a Coherent FieldMaster powermeter with an LM-10HTD measuring head.

Parameters of the bubbles shown in Fig. 3

	Parameters of radiation			
	CW radiation, 3 W (Fig. 3a)		pulsed radiation, 6 W (Fig. 3b)	
	diameter, μm	velocity, mm/s	diameter, μm	velocity, mm/s
1	26	9	17	38
2	26	9	10	37
3	200	3	10	5
4	58	16	41	60
5	42	12	21	20
6	63	48	21	52
7	47	97	27	32

RESULTS AND DISCUSSION

The laser energy is partly (10–20%) absorbed in the carbon layer on the blackened fiber, so that the fiber is heated. When the laser radiation with a power of greater than 3 W is transmitted by the fiber end in air, the spectrum of the optical radiation from the fiber end contains the fundamental line (970 or 1550 nm) and the broadband visible and near-IR radiation related to the heating of the end surface to relatively high temperatures. When the blackened end is placed in water, the end surface is effectively cooled and the absence of the broadband radiation indicates substantially lower temperatures of the end surface. However, the laser radiation with moderate power (1–5 W) is sufficient for the heating of the end surface and the generation of gas–vapor bubbles. When water is heated, the dissolved gases are liberated in the vicinity of the end surface and gas bubbles emerge. Water is evaporated inside the bubbles, so that the bubbles are filled with vapor and, consequently, increase in size. At the lower boundary of the above power interval, the bubbles increase in size residing on the end surface. When a critical size is reached, the bubbles are detached and rise to the surface (Fig. 1a). Water molecules that approach the heated end surface acquire additional kinetic energy and momentum. The component of the total momentum of vapor molecules that is directed perpendicularly to the end surface of the fiber towards water appears insufficient for the detachment of the bubble. Figure 1a shows that the sizes of bubbles can be close to the diameter of the quartz core (400 μm). In the experiments, the bubbles normally emerge at the same spots on the end surface, which

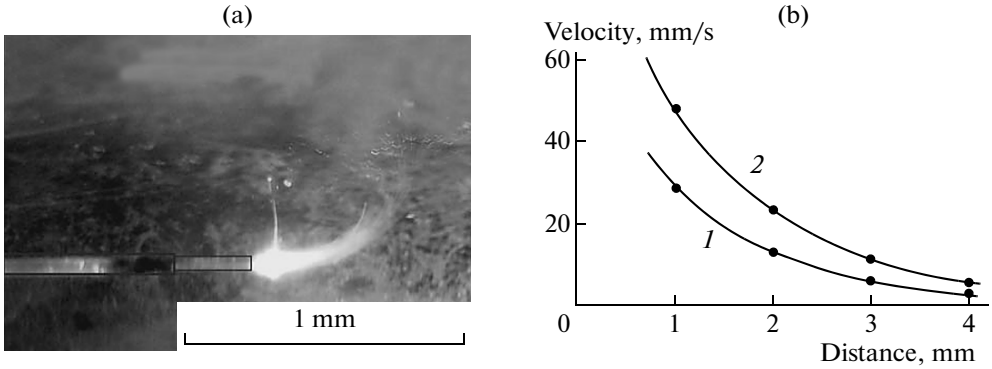

Fig. 2. (a) Side view of the tracks of microbubbles in the vicinity of the blackened end surface of the optical fiber in water and (b) plots of the horizontal velocity vs. distance from the end surface for (*1*) slowest and (*2*) fastest bubbles at a laser wavelength of 970 nm and a power of 5 W.

must be the high-temperature areas. Evidently, the presence of such spots is related to the nonuniformity of the carbon layer with respect to thickness: the absorbed energy (and, hence, the temperature) is greater for thicker regions. The stabilization (i.e., the attachment of the gas–vapor bubbles to the high-temperature spots) can be due to two reasons. First, the temperature at the hot spot additionally increases owing to the formation of the bubble and the consequent decrease in the local heat sink to water. The second reason is related to the Marangoni effect [12]: the temperature gradient gives rise to the gradient of surface tension, so that the convective flows emerge on the surface of the bubble and cause the force that presses the bubble to the hot spot. The experiments on the growth of the bubbles in the vicinity of the end surface show that the rate of growth gradually decreases and, finally, the growth is terminated. At a laser power of 1 W, the duration of a relatively fast growth is about 200 ms. At this stage, the size of the bubble increases from zero to 25% of the maximum size. Then, over a few seconds, the growth is well described with the dependence $D \propto t^{4/5}$, where D is the diameter of bubble and t is time. When the laser irradiation is terminated (Fig. 1a), the size of bubble gradually decreases (the bubble remains attached to the end surface of the fiber) and, finally, the bubble vanishes. Note that a decrease in the size is also nonmonotonic. At the first stage with a duration of less than 1 s, the diameter decreases by 8–10%. Then, the slowing takes place, so that a diameter of 300–400 μm additionally decreases by 1% over an interval ranging from 15 min to 2.5 h. Such a nonmonotonic behavior must be related to the fact that the size of bubble decreases at the first stage predominantly due to a decrease in the temperature of the gas–vapor mixture inside the bubble to the temperature of water in the cell, whereas the second stage is isothermal. The lifetime of such bubbles ranges from 3 to 8 h, and the rate of a decrease in the diameter with time always monotonically increases. At the second stage, the dependence of the diameter on time is well approximated with the expression $D = D_0(1 - t/\tau_0)^\alpha$, where D_0 is the initial diameter, τ_0 is lifetime, and $\alpha = 0.1–0.5$ is the empirical parameter. Note a similar decrease in the diameter with time at $\alpha = 0.5$ in [13].

A qualitatively different scenario corresponds to higher laser powers. The explosive boiling of water is observed in the vicinity of the hot end: the gas–vapor bubbles are ejected from the fiber to water (Fig. 1b) and, then, the velocity decreases due to viscosity. At a finite exposure time, we observe the tracks of bubbles moving in water. Note that the track length corresponds to the mean velocity of the bubble over the exposure time and the track thickness corresponds to the size of bubble. Bright spots in the vicinity of the end surface (Fig. 1) are related to stray light: the Vision video camera is sensitive to the near-IR laser radiation.

The side measurements (Fig. 2a) show that the bubbles come to the surface at a certain distance from the fiber. Knowing the vertical velocity of the bubbles (about 5 mm/s in accordance with visual observations) and the trajectories, we can estimate the horizontal velocity (Fig. 2b). The analysis of the trajectories yields an exponential decrease in the horizontal velocity with increasing distance from the fiber: for the slowest and fastest bubbles, we obtain the dependences $v = 67\exp(-0.82r)$ and $v = 101\exp(-0.74r)$, respectively, where v is the horizontal velocity in mm/s and r is the distance from the end surface in millimeters. The relationships show that the velocity of bubbles at the moment of the detachment from the fiber end ($r = 0$) ranges from 67 to 101 mm/s.

In the experiments on the generation of microbubbles in the vicinity of the end surface of the quartz fiber performed with the aid of the Photron Fascam SA3 (Fig. 3), we directly observe the motion of bubbles even in the immediate vicinity of the end surface (at the maximum velocities). Figure 3 shows the bubbles as dark circles with different sizes. The previous (at time step Δt) positions and sizes are shown as open cir-

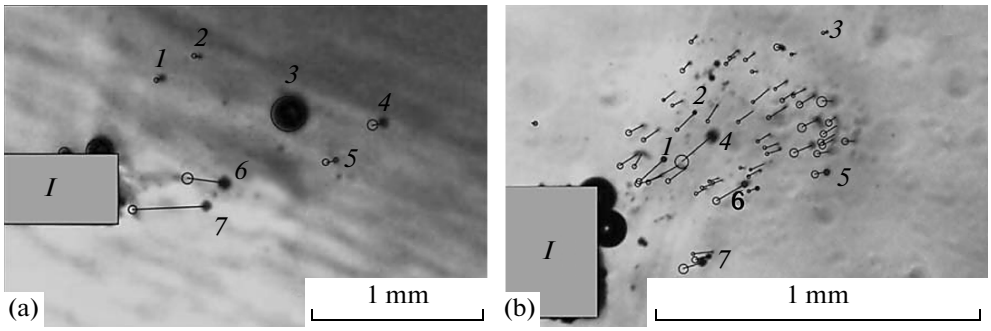

Fig. 3. Displacements of microbubbles (that are generated in the vicinity of the schematically shown blackened end surface of quartz fiber *I*) over short time intervals Δt in the presence of (a) CW and (b) pulsed laser radiation: (closed circles *1*–*7*) positions of bubbles, (open circles) previous positions, and (rectilinear segments) trajectories. The images are taken from above at rates of (a) 10000 and (b) 2000 frames per second, laser powers of (a) 3 and (b) 6 W, time intervals Δt = (a) 4.4 and (b) 2.0 ms, and a laser wavelength of 970 nm (the pulse duration is 50 ms and the interval between pulses is 500 ms).

cles, and the trajectories are shown as rectilinear segments. Table presents the calculated sizes and velocities of the bubbles shown in Fig. 3. It is seen that the bubble with a diameter of 47 μm (bubble *7* in Fig. 3a), which is located at a distance of about 100 μm from the fiber end at the initial moment, moves at a mean velocity of 97 mm/s over the observation interval (4.4 ms). This result is in good agreement with the above estimations of the initial velocities in the vicinity of the fiber end. The velocities of the bubbles rapidly decrease with increasing distance from the fiber: the velocities are no greater than 50 and 20 mm/s at distances of 500 μm and 2 mm, respectively. When the bubbles are generated over a relatively long time interval in a viscous liquid, a steady-state flow results in an increase in the velocities of bubbles relative to a stationary observer. To determine the relative contribution of such a flow, we measure the motion of microbubbles under the pulsed laser irradiation (Fig. 3b). It is seen that the bubbles predominantly move at relatively large angles relative to the fiber axis. This result must be due to the features of the end surface and hydrodynamic effects. Note that the asymmetry also corresponds to the motion of microbubbles under the CW irradiation. Figure 3b shows that a short laser pulse with a pulse power of 6 W causes the generation of many bubbles whose diameters range from 10 to 41 μm. The velocities of bubbles are 60 and 20 mm/s in the vicinity of the fiber and at a distance of 800 μm, respectively. In spite of a twofold increase in the laser power, the maximum velocities of the bubbles in the vicinity of the fiber under the pulsed irradiation are significantly less than the velocities corresponding to the CW irradiation. At a relatively large distance from the fiber end, the velocities corresponding to the pulsed irradiation are also less than the velocities corresponding to the CW irradiation: the velocity of bubble *4* in Fig. 3 is almost equal to the velocity of bubble *5* in Fig. 3b, whose distance from the fiber end is almost two times smaller (table). This result indicates the presence of flows in the case of the CW irradiation and shows that the flow velocity is comparable with the mean velocity of bubbles.

Such liquid flows are more clearly observed in the microscopic measurements of the laser-induced hydrodynamic effects in the vicinity of the end surface of the fiber that is placed in the glass capillary filled with water (model of the laser channel) (Fig. 4). At a power of 1–2 W, the attached gas–vapor bubbles emerge at the end surface and the convective motion is observed in the liquid. A qualitatively different scenario corresponds to a power of 3 W: the microscopic bubbles ejected from the fiber end move along arc-shaped trajectories and entrain liquid flows (Fig. 4a). The intensity of the resulting vortices rapidly increases with increasing radiation power (Fig. 4b). In accordance with the estimations based on the frame-to-frame analysis of the video records, the period of the typical circulating liquid flows at laser powers of 3–5 W ranges from 0.2 to 1.0 s.

Note that the above effects can be observed in the experiments with the blackened fiber end at both laser wavelengths (970 nm and 1.55 μm). In the absence of the preliminary blackening, the effects are observed only for a radiation wavelength of 1.55 μm. Such a difference is related to the fact that the radiation with a wavelength of 1.55 μm (unlike the short-wavelength radiation) is capable of heating a thin water layer in the vicinity of the end surface to the boiling point, since the absorbance at a wavelength of 1.55 μm is greater than the absorbance at a wavelength of 970 nm by a factor of about 20 [14].

Note an interesting phenomenon in the experiments on the generation of bubbles in the vicinity of the blackened end surface of the fiber in the water cell: bubble microjets can be generated at a laser power of less than 3 W (Fig. 5). The lengths of the jets, which always start in the immediate vicinity of the fiber end, reach several millimeters, the transverse sizes normally range from 10 to 50 μm, and the sizes of the bubbles that form the jets range from several to ten microns.

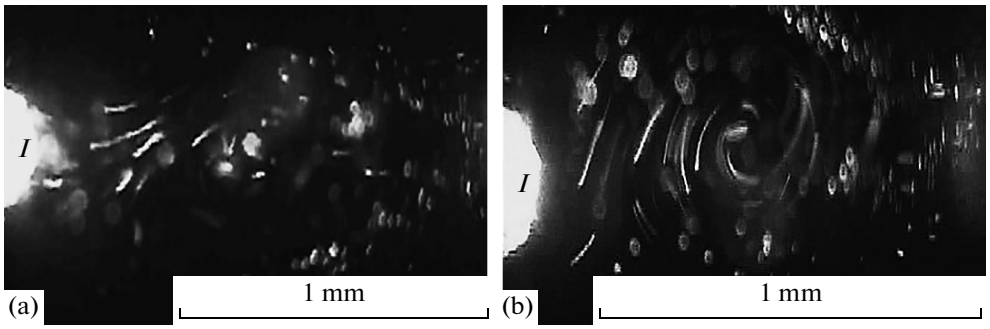

Fig. 4. Water flows that actively circulate inside the glass capillary (with a diameter of 1 mm) in the vicinity of the blackened end surface *I* heated by the laser radiation with a wavelength of 970 nm and a power of (a) 3 and (b) 5 W (the photographs are taken from above).

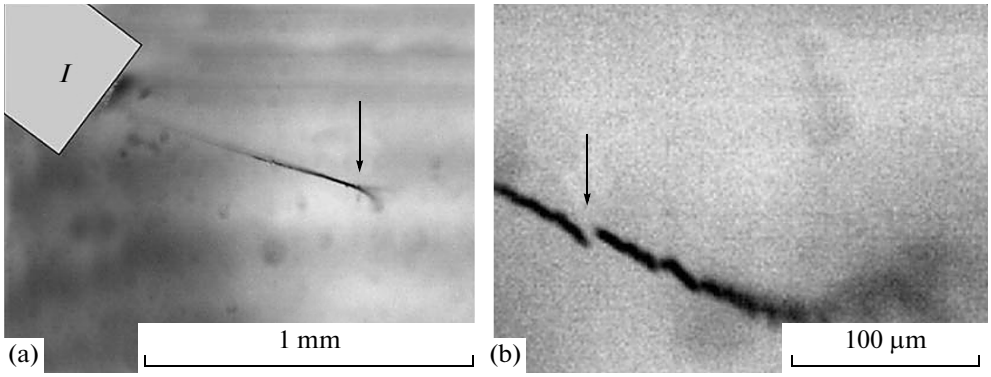

Fig. 5. Bubble microjets in the vicinity of the schematically shown end surface of the optical fiber *I*. Arrows show the points where the jets loose stability.

The lifetime of the jets ranges from a few fractions of a second to tens of seconds. A jet that emerges at a certain spot on the end surface remains attached to this spot and exhibits bending relative to the mean position. Note the discontinuities (arrow in Fig. 5b) and the subsequent recovery of the jet. The observations show that the discontinuities are always related to the hydrodynamic perturbations and are caused by relatively large bubbles that move in the vicinity of the jet. Thus, we conclude that two conditions must be satisfied for the generation of the jets. First, a hot spot must be formed on the end surface for the generation of the jet. Second, the neighborhood of such a spot must be free of the centers that provide the generation and detachment of large bubbles. Note that the possibility of bubble microjets in the vicinity of a point heat source is demonstrated in [13].

Thus, the hydrodynamic processes related to the explosive boiling in the vicinity of the hot end surface are observed in the liquid even at moderate laser powers. Note that the intracapillary liquid exhibits effective mechanical oscillations with a frequency of 1–5 Hz and appears saturated with microbubbles. We expect the development of such laser-induced hydrodynamic processes in water-saturated biotissues at moderate laser powers. On the one hand, such processes provide the saturation of cavities and fractures in a disk or bone with the water solution containing gas–vapor bubbles. On the other hand, they give rise to high-power acoustic oscillations and vibrations in the organ containing the connective tissue. Apparently, the filling of hernia with gas–vapor bubbles provides the reproducible decrease in the density of herniation immediately after the laser treatment [5]. It is known from [4] that the mechanical action on cartilages in the hertz frequency range actively stimulates the synthesis of collagen and proteoglycans even at relatively small amplitudes. The above estimations show that the pressure on biotissue provided by the gas–vapor bubbles can reach tens of kilopascals. In accordance with [15, 16], such pressures in the hertz frequency range can lead to regenerative processes in cartilage owing to the activation of the interaction of the extracellular matrix with the mechanoreceptors of chondrocytes (integrins).

CONCLUSIONS

We study the hydrodynamic effects induced by the moderate-power (1–5 W) laser radiation in the vicinity of the heated end surface of the optical fiber in water. We perform the measurements in bulk liquid and in the glass capillary that simulates the laser channel. A developed threshold character of the dynamics of liquid is demonstrated. At a relatively low laser power (about 1 W), we observe the slow formation of gas–vapor bubbles with sizes of hundreds of microns on the end surface of the optical fiber. The bubbles can be attached to the end surface during the irradiation session. When the laser power increases, we observe the effective hydrodynamic processes related to the explosive boiling in the vicinity of the hot end surface. The resulting bubbles with sizes ranging from a few microns to several tens of microns provide the motion of liquid. The estimations yield a velocity of up to 100 mm/s for the bubbles in the vicinity of the end surface. The generation of bubbles in the capillary leads to the circulating liquid flows with periods ranging from 0.2 to 1.0 s. Note that the circulation intensity increases with the laser power. For the laser radiation with a wavelength of 0.97 μm, we observe such effects only for the blackened end surface of the quartz fiber, which serves as a point heat source. At a laser power of less than 3 W, stable bubble microjets, which consist of the bubbles whose sizes range from several to ten microns, can be generated in the vicinity of the blackened end surface. The above hydrodynamic effects can be involved in the surgical procedures and can stimulate the regeneration processes.

In the further experiments, we will study the laser-induced hydrodynamic processes in biotissues and optical delivery fibers.

ACKNOWLEDGMENTS

This work was supported by the Russian Foundation for Basic Research (project no. 09-02-00714).

REFERENCES

1. H. P. Berlien and G. Muller, *Applied Laser Medicine* (Springer, Heidelberg, 2003).
2. S. N. Joffe, Surg. Endoscopy **1**, 25 (1987).
3. C. K. Rokhsar and D. H. Ciocon, Dermatol. Surg. **35**, 535 (2009).
4. *Laser Engineering of Cartilage* (Fizmatlit, Moscow, 2006).
5. B. I. Sandler, L. N. Sulyandziga, V. M. Chudnovskii, V. I. Yusupov, O. V. Kosareva, and V. C. Timoshenko, *Prospects for Treatment of Compression Forms of Discogenic Lumbosacral Radiculitis by Means of Puncture Nonendoscopic Laser Operations* (Dalnauka, Vladivostok, 2004).
6. B. I. Sandler, L. N. Sulyandziga, V. M. Chudnovskii, V. I. Yusupov, and Y. M. Galin, Bull. Physiol. Pathol. Breath **11**, 46 (2002).
7. V. M. Chudnovskii and V. I. Yusupov, "Method of Laser Intervention Effects in Osteochondrosis," Patent RF No. 2321373, Byull. Izobret. No. 10 (2008).
8. V. A. Privalov, I. V. Krochek, and A. V. Lappa, Proc. SPIE **4433**, 180 (2001).
9. A. I. Shnirel'man, E. N. Sobol', and V. N. Bagratashvili, Laser Phys. **14**, 1 (2004).
10. E. N. Sobol, T. E. Milner, A. B. Shekhter, O. I. Baum, A. E. Guller, N. Y. Ignatieva, A. I. Omelchenko, and O. L. Zakharkina, Laser Phys. Lett. **4**, 488 (2007).
11. T. G. Leighton, *The Acoustic Bubble* (Academic, London, 1994).
12. D. W. Berry, N. R. Heckenberg, and H. Rubinszteindunlop, J. Mod. Opt. **47**, 1575 (2000).
13. R. S. Taylor and C. Hnatovsky, J. Appl. Phys. **95**, 8444 (2004).
14. G. M. Hale and M. R. Querry, Appl. Opt **12**, 555 (1973).
15. M. D. Buschmann, Y. A. Gluzband, A. J. Grodzinsky, and E. B. Hunziker, J. Cell Sci. **108**, 1497 (1995).
16. S. J. Millward-Sadler and D. M. Salter, Ann. Biomed. Eng. **32**, 435 (2004).